Contents lists available at SciOpen

Food Science and Human Wellness

journal homepage: https://www.sciopen.com/journal/2097-0765

Structural characterization and anti-inflammatory activities of novel polysaccharides obtained from *Pleurotus eryngii*

Han Wang[a], Sai Ma[a], Alfred Mugambi Mariga[b], Qiuhui Hu[a], Qian Xu[a], Anxiang Su[a], Ning Ma[a], Gaoxing Ma[a,*]

[a] *College of Food Science and Engineering, Nanjing University of Finance and Economics/Collaborative Innovation Center for Modern Grain Circulation and Safety, Nanjing 210023, China*
[b] *School of Agriculture and Food Science, Meru University of Science and Technology, Meru 972-60200, Kenya*

ARTICLE INFO

Article history:
Received 2 May 2023
Received in revised form 17 May 2023
Accepted 3 June 2023

Keywords:
Pleurotus eryngii
Polysaccharides
Structural characterization
Anti-inflammatory activity

ABSTRACT

Natural polysaccharides named PEP-0.1-1, PEP-0-1 and PEP-0-2 from edible mushroom species *Pleurotus eryngii* were obtained in the present study. Results showed that molecular weights of these polysaccharides were 3 235, 2 041 and 23 933 Da, respectively. Further, structural characterization revealed that PEP-0.1-1 had a →4-*α*-*D*-Glc*p*-1→ backbone and contained →4)-*α*-*D*-Glc*p* and →4)-*β*-*D*-Glc*p* reducing end groups. PEP-0-1 backbone contained→4-*α*-*D*-Glc*p*-1→ and →6-*α*-3-*O*-Me-*D*-Gal*p*-1→, and the side chains contained *α*-*D*-Glc*p*, *β*-*D*-Man*p*-1→ and *α*-*D*-Glc*p*-3→. However, PEP-0-2 backbone consisted of →4-*α*-*D*-Glc*p*-1→ and →6-*α*-3-*O*-Me-*D*-Gal*p*-(1→6)-*α*-*D*-Gal*p*-1→ while the side chains contained *α*-*D*-Glc*p* and *β*-*D*-Man*p*-1→. Biological activity analysis was then carried out and found that all these polysaccharides could significantly suppress the relative mRNA expression of toll-like receptor 4, nitric oxide (NO), tumor necrosis factor-α, interleukin (IL)-1β and IL-6 in lipopolysaccharide (LPS)-induced inflammation of RAW264.7 cells, as well as the over secretion of the above cell cytokines. Moreover, Western blotting analysis revealed that all these purified fractions displayed significant inhibition effects on the expression of c-Jun N-terminal kinases protein induced by LPS in mitogen activated protein kinase pathway, along with the relieving on the inhibition effect of LPS on IκB-α protein expression. In summary, the information generated by the present study could provide a theoretical basis for the exploration of novel healthy food materials from edible mushroom with anti-inflammation activities.

1. Introduction

Polysaccharides from edible fungi were active macromolecules which have been intensively studied and proved displaying a great efficacy and prospects in the improvement of metabolic syndrome illnesses when utilized as nutritional dietary supplements[1-2]. As one of the most cultivated and consumed edible mushrooms all around the world, *Pleurotus eryngii* has been proved exhibiting high nutritional value and various biological activities due to its multiple bioactive components, such as polysaccharides, polyphenols, proteins, minerals and vitamins[3-4]. Specifically, *P. eryngii* polysaccharide represented diversity in its biological activities, mainly including hypotensive, antibacterial, anti-inflammatory, antiviral, anti-diabetes, hypolipidemic, anti-tumor, immunomodulatory and anti-oxidation activities[5-7], from which its anti-inflammatory activity has been proved one of the most significant biological features.

Generally, inflammation was considered a defensive immune response to cell cytokines[8]. As one of the important defense barriers in the human immune systems, innate immune system was regarded as the most rapid response to pathogens invasion. Pattern recognition receptors in the innate immune system of the host recognize the invasion signal whereby they activate the inflammatory signaling pathway, induce the production of pro-inflammatory cytokines and cause inflammatory response[9]. However, excessive inflammation reflection demonstrated significant damage to body health, leading to stroke, rheumatoid arthritis, neurodegenerative diseases and

* Corresponding author at: College of Food Science and Engineering, Nanjing University of Finance and Economics, Nanjing 210023, China.
E-mail address: magaoxing90@163.com (G.X. Ma)
Peer review under responsibility of Tsinghua University Press.

Publishing services by Tsinghua University Press

http://doi.org/10.26599/FSHW.2022.9250245

cardiovascular diseases[10]. Basically, all of these revealed adverse reaction could not be ignored, from which resulted the promotion of using traditional strategies for inflammation improvement, mainly including the specific drugs or functional foods with anti-inflammatory bioactivities[11]. At present, studies have demonstrated that *P. eryngii* polysaccharides have anti-inflammatory activity[12]. Silveira et al.[13] studied the structure and anti-inflammatory activity of a kind of *P. eryngii* extracellular polysaccharide (EPS), the results showed that EPS was mainly contained mannose and galactose. Pain and edema were 2 features of the inflammatory process. *In vitro* experiments, EPS could significantly reduce the foot edema of mice, and the results strongly indicate that EPS has significant anti-inflammatory activity and can be used as an anti-inflammatory agent. Therefore, we speculated that the purified *P. eryngii* polysaccharide could be ideal candidate for novel functional food development and aimed to reveal its specific structural characteristics, as well as the related anti-inflammatory effects and potential mechanisms in this study.

Based on the previous studies, the functional and nutritional properties of *P. eryngii* polysaccharides were closely correlated with its specific structural characteristics[14]. Herein, it is essential and pivotal to analyze its elaborate structural characteristics, from which the generated results could be beneficial for the utilization of *P. eryngii* polysaccharide to achieve precision development of novel functional foods with different activities. On the other side, previous studies have revealed the primary structures of *P. eryngii* polysaccharide, which were mainly including the monosaccharide composition, molecular weight, functional group type and monosaccharide linking mode. However, its fine structure characteristics has not been illustrated[15].

Herein, fine structures of purified polysaccharides obtained from *P. eryngii* were detected in the present study, as well as the related anti-inflammatory activities and functional mechanisms. Results of this research could provide theoretical foundation for the development and application of novel edible mushroom-derived functional components with anti-inflammatory activities.

2. Materials and methods

2.1 Materials and reagents

Fresh *P. eryngii* powder was purchased from a local commercial supermarket (Nanjing, China). Cellulose DE-52 and Sephadex G-100 medium were obtained from Solarbio Science & Technology Co., Ltd., (Beijing, China). While cells utilized in the study were purchased from Procell Life Science & Technology Co., Ltd., (Hubei, China). Fetal calf serum (FBS) was purchased from Gibco Life Technologies (Grand Island, NY, USA), Cell Counting Kit-8 (CCK-8) and nitric oxide determination kit were acquired from Beyotime Biotechnology (Shanghai, China) whereas other ELISA kits were procured from Jiancheng Bioengineering Institute (Nanjing, China). Moreover, standard monosaccharides were obtained from Putian Tongchuang Biotechnology (Beijing, China).

2.2 P. eryngii polysaccharides preparation

The process for *P. eryngii* polysaccharides preparation was carried out based on a preliminary experiment. Basically, dried *P. eryngii* powders were defatted using 85% ethanol (1:15, *m*/*V*) at 25 °C for 12 h. Distilled water was then added to the precipitate (solid-liquid ratio, 1:36 g/mL). An ultrasonic cleaner equipped with a digital timer, temperature and power controller was used to degrade *P. eryngii* powder, whereby, the reaction was maintained at 38 °C for 30 min (output power was 464 W; frequency was 80 kHz), followed by an extraction process (distilled water; temperature was 60 °C and extraction time was 3.5 h). The resultant aqueous solution was then centrifuged and concentrated to a third of the original volume and precipitated using three times volume of 95% ethanol for 12 h at a room temperature. Finally, the obtained precipitate was deproteinated using the Sevag method[16]. The Sevag reagent was then removed from the solution by dialysis. After dialysis, the sample was concentrated and freeze-dried to acquire the initial polysaccharide fraction, which was denoted PEP. Then 100 mg of PEP was later re-dissolved in 20 mL of ultrapure water, passed through cellulose DE-52 column, and sequentially eluted with ultrapure water, 0.1 and 0.3 mol/L NaCl solutions at 1.0 mL/min (10 mL/tube) elution velocity, the obtained components were named PEP-0, PEP-0.1, and PEP-0.3, respectively. Next, the obtained fractions were dialyzed, lyophilized, and stored for further analysis. Afterwards, 50 mg freeze-dried samples (PEP-0, PEP-0.1, and PEP-0.3) were re-dissolved in 20 mL of ultrapure water, respectively. Then passed through a G-100 Sephadex gel-filtration column (eluate was distilled, velocity was 0.25 mL/min; 10 mL/tube). Finally, lyophilization was done to obtain the final purified polysaccharides fractions.

2.3 Characterization of PEP

2.3.1 Ultraviolet-visible (UV-vis) spectroscopy assay

The absorbance of the purified polysaccharides (0.5 mg/mL) were read within a wavelength range of 200−400 nm using UV-2401PC spectrophotometer (Shimadzu, Japan). Subsequently, the appearance of absorption peaks at 260 and 280 nm were observed and utilized to ascertain whether the samples contained nucleic acids and proteins[17].

2.3.2 Fourier-transform infrared spectra (FT-IR) analysis

Five mg of dried purified polysaccharides and KBr powder were lightly ground in a mortar, and the mixture pressed into thin tablets by a tablet press. The samples were then scanned in a FT-IR (Thermo Fisher, USA) at a wavelength range of 4 000−500 cm^{-1} with a resolution of 2 cm^{-1} [18].

2.3.3 Analysis of monosaccharide compositions

Monosaccharides profile of *P. eryngii* polysaccharides was determined based on the previous published protocol[19]. A detailed process was presented in Supplementary method 1.

2.3.4 Determination of molecular weights

Standard glucan solutions (1 mg/mL) with different molecular weights and polysaccharide solutions (2 mg/mL) were prepared and analyzed by Agilent 1200 series high performance liquid chromatography (Agilent, USA) equipped with a TSK-GEL G4000 SWXL column (300 mm × 7.8 mm) and an evaporative light detector (ELSD) at a column and detector temperature of 25 °C and a mobile

phase flow rate of 0.6 mL/min[20].

2.3.5 Methylation analysis

In the present study, methylation of the obtained purified polysaccharide fractions was analyzed using an earlier reported method with some modifications[21]. A detailed process was presented in Supplementary method 2.

2.3.6 Nuclear magnetic resonance (NMR) analysis

Firstly, 30 mg samples (PEP-0.1-1, PEP-0-1, PEP-0-2) were dissolved in 0.5 mL of heavy water, respectively. Then followed with lyophilization. The obtained samples were re-dissolved in 0.5 mL heavy water and refreeze-dried. Secondly, the freeze-dried samples were dissolved in 0.5 mL heavy water, and analyzed in a 600 MHz nuclear magnetic resonance instrument (Bruker, Rheinstetten, Germany) at 25 °C to determine the ^{1}H NMR, and ^{13}C NMR spectrum, as well as the correlation spectroscopy (COSY), heteronuclear single-quantum coherence (HSQC), heteronuclear multiple bond correlation (HMBC), and nuclear Overhauser effect spectroscopy (NOESY) spectra[22].

2.4 Anti-inflammatory activities of P. eryngii polysaccharides

2.4.1 Cell culture and establishment of the lipopolysaccharide (LPS)-induced inflammation model

RAW264.7 cells were cultured in a 5% CO_2 incubator at 37 °C with complete culture medium containing DMEM, 10% fetal bovine serum and 1% penicillin-streptomycin. The cells (2×10^5 cells /mL) were then inoculated into 24-well cell culture plates and cultured for 12 h, after which, the used medium was replaced with fresh DMEM medium containing different concentrations of polysaccharides (5, 10 and 25 μg/mL), each well contained 200 μL DMEM. After 4 h of culturing, the old culture medium was discarded and fresh DMEM medium with or without LPS (100 ng/mL) was added and further incubated for 24 h, each well contained 20 ng LPS. The culture wells contained only culture medium (no polysaccharide or LPS) were used as blank control whereas, culture wells contained cells and LPS were used as negative control. CCK-8 was utilized for the determination of cell viability in different groups.

2.4.2 Quantitative reverse transcription polymerase chain reaction (qRT-PCR)

Cell suspension was collected, mixed with 1 mL Trizol reagent and 200 μL chloroform, followed with centrifugation (12 000 r/min, 4 °C and 15 min). RNA was then mixed with isopropanol of equal volume. Subsequently, the mixture was placed in a refrigerator at −20 °C for 20−30 min followed by centrifugation at 12 000 r/min at 4 °C for 5 min and excess isopropyl alcohol discarded. Next, 1 mL of cold 75% ethanol was added to the precipitate followed by centrifugation at 12 000 r/min, 4 °C for 5 min. After centrifugation, the supernatant and the excess ethanol were discarded. On complete ethanol volatilization, 50−100 μL Rnase-free double stilled water (ddH_2O) was added into a centrifuge tube and the concentration and purity determined by micronucleic acid protein analyzer. Following the manufacturer's instructions, Vazyme reverse transcription kit was used for reverse transcription reactions.

2.4.3 Secretion of toll-like receptor 4 (TLR4), nitric oxide (NO), tumor necrosis factor (TNF)-α, interleukin (IL)-1β and IL-6

A volume of 200 μL of a cell suspension (2×10^5 cells/mL) was loaded into each well of a 96-well plate to achieve a cell density of 4×10^4 cells/well and treated as described above. Then, the concentrations of TLR4, NO, TNF-α, IL-1β and IL-6 in the culture medium supernatant of different groups were detected using kits according to the manufacturer's instructions.

2.5 Western blotting

RAW264.7 cells were treated as described in section 2.4.1, and the culture medium was discarded after 24 h. Then, cells were washed twice with PBS and lysed with RIPA lysate solution at 4 °C. Afterwards, the lysates were collected and centrifuged at 10 000 r/min for 5 min. Protein contents in the supernatant was determined by BCA kit. Proteins were denatured by boiling water bath, and were separated in 12% sodium dodecyl-sulfate polyacrylamide gel electrophoresis (SDS-PAGE) subsequently, followed with the transferring process on 0.45 μm PVDF membranes. Then, PVDF membranes were incubated with primary antibody overnight at 4 °C, and washed 3 times with Western detergent, blocked with skim milk for 4 h, washed 3 times with Western detergent, incubated with corresponding secondary antibody for 2 h at room temperature, then washed 3 times with Western detergent. At last, antibody-specific proteins were visualized with ECL enhancement kit and photographed with chemiluminescence imaging system.

2.6 Statistical analysis

Results were expressed as mean values and standard deviation (SD). Statistical analyses were performed using SPSS statistical software and statistical significance was defined as $P < 0.05$.

3. Results and discussion

3.1 solation and purification of PEP

The overall procedure for the present study was schematically presented in Fig. 1A. Essentially, 4.4% of crude PEP with a carbohydrate content of 44.4% was obtained. After purification through cellulose DE-52 column, the eluted solution was separated into 3 fractions named PEP-0, PEP-0.1 and PEP-0.3, respectively (Fig. 1B). Nevertheless, due to the extremely low recovery rate of PEP-0.3, PEP-0.3 was not collected for subsequent experiments, thus the fractions, PEP-0 and PEP-0.1 were collected and subjected to further purification. On subsequent purification of fraction PEP-0, two main peaks were yielded; PEP-0-1 and PEP-0-2, which had a sugar content of 99.28% and 97.59%, respectively. Following further purification of fraction PEP-0.1, a consequent pure fraction named PEP-0.1-1 was obtained which in turn had a sugar content of 99.42%. The eluent curves of fractions PEP-0 and PEP-0.1 were showed in Figs. 1C and D, respectively.

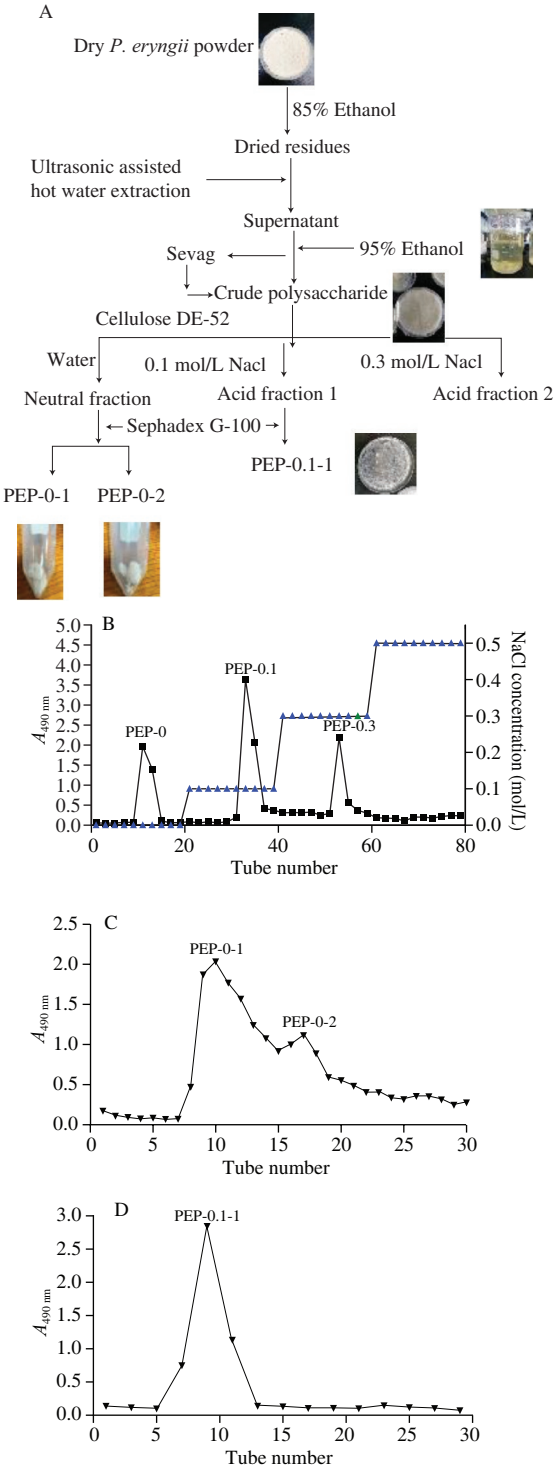

Fig. 1 Extraction and isolation of PEP from *P. eryngii*. (A) PEP extraction and isolation scheme; (B) PEP elution curve on cellulose DE-52 column; (C) Elution curve of PEP-0 on Sephadex G-100 column; (D) PEP-0.1 elution curve on Sephadex G-100 column.

3.2 Structure analysis of purified *P. eryngii* polysaccharides

3.2.1 UV analysis

There was no optical absorption peak at 260 and 280 nm, which indicated that neither proteins nor nucleic acids were present in the purified fractions (Fig. 2).

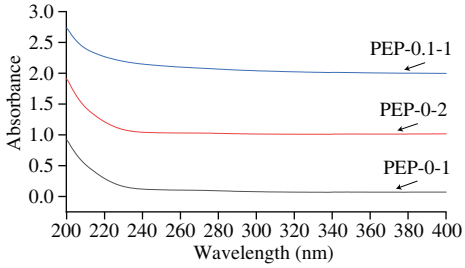

Fig. 2 UV-vis spectra of PEP-0.1-1, PEP-0-2 and PEP-0-1 from 200 to 400 nm.

3.2.2 FT-IR analysis

The structure of polysaccharides could be identified by infrared spectroscopy based on the interpretation of absorption peaks at a specific wavenumber[23]. Hence, infrared spectral scanning was performed for the 3 purified polysaccharides, as shown in Fig. 3. The O−H vibration of the 3 polysaccharides generated a peak at 3 396 cm^{-1}, which was typical for carbohydrates. Additionally, an absorption peak was observed at 2 937 cm^{-1} which was due to the contraction vibration of methyl C−H functional group in polysaccharides[24]. Besides, the specific peak observed at 1 636 cm^{-1} was mainly due to the asymmetric C=O stretching vibrations, it's probably caused by vibrations of the carboxyl group (−CHO) in the sugar ring[25]. In addition, a peak was observed at 1 423 cm^{-1}, which was as a result of C−H bending vibration. Moreover, the peak, 1 249 cm^{-1} observed for the 3 polysaccharides was attributed to methyl acetyl group (CH_3)[26]. The fingerprint region between 1 200 to 800 cm^{-1} reflected the differences in the polysaccharide's structure and monosaccharides composition[27]. Furthermore, the peaks in the region 1 000–1 200 cm^{-1} were attributed to the contraction vibrations of C−O−C glycosidic bond and C−O−H side chain functional groups, indicating the existence of pyranose rings in the three polysaccharides.

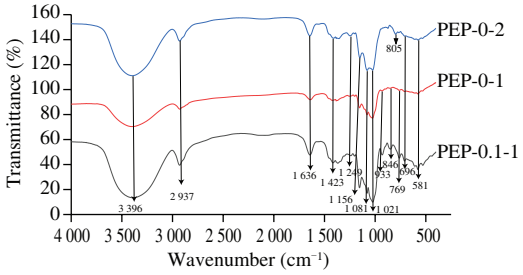

Fig. 3 FT-IR spectra of PEP-0.1-1, PEP-0-1 and PEP-0-2 from 4 000 to 400 cm^{-1}.

3.2.3 Monosaccharide composition and molecular weight

Results on the molecular weight determination revealed that the 3 polysaccharide fractions were homogeneous. On the other hand, results on the monosaccharide composition (Fig. 4) indicated that the three fractions were mainly abundant in glucose. Specifically, PEP-0.1-1 contained galactose and glucose at a 6.63:93.37 ratio and had a molecular weight (*Mw*) of 3 235 kDa whereas PEP-0-1, with a *Mw* of 2 041 kDa, contained fructose, galactose, glucose, xylose, mannose, and fructose at a 0.14:0.73:94.2:0.61:2.79:1.53 ratio respectively. Besides, PEP-0-2, which had a *Mw* of 23 933 Da, contained fructose, galactose, glucose, xylose and mannose at a 0.64:16.62:68.56:0.51:13.67 ratio respectively, as shown in Fig. 5.

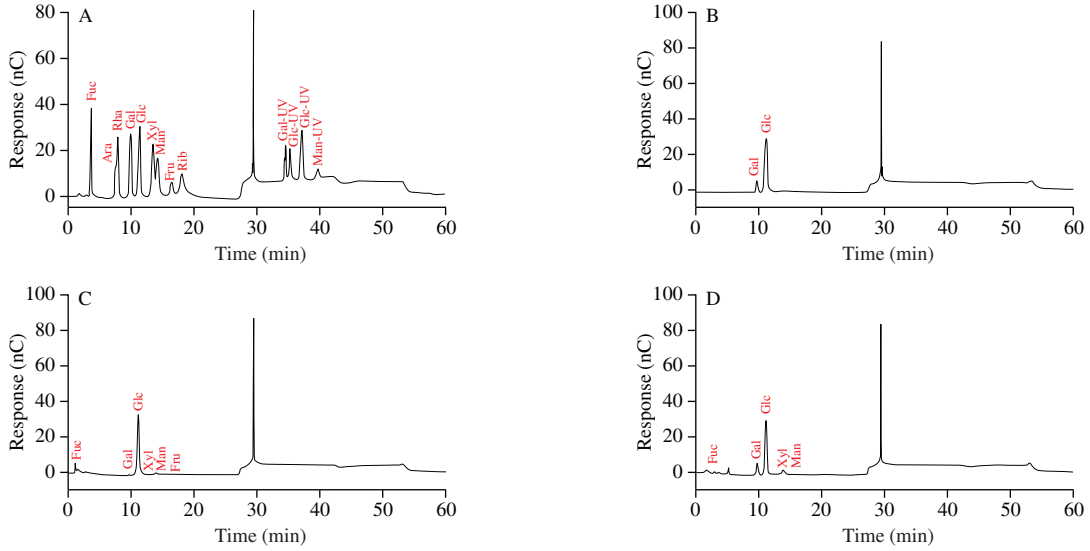

Fig. 4 Monosaccharide composition of (A) sugar standard mixture, (B) PEP-0.1-1, (C) PEP-0-1 and (D) PEP-0-2. Fuc, fructose; Ara, arbinose; Rha, rhamnose; Gal, galatose; Glc, glucose; Xyl, xylose; Man, mannose; Fru, fructose; Rib, ribose.

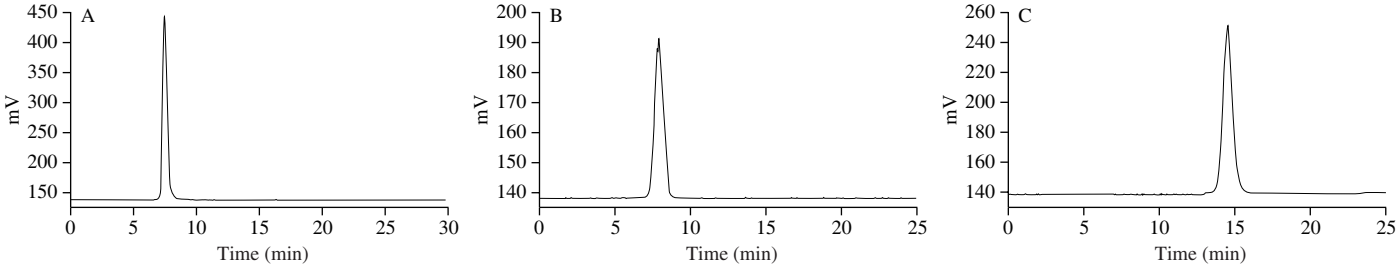

Fig. 5 Molecular weight distribution of polysaccharide samples (A) PEP-0.1-1, (B) PEP-0-1 and (C) PEP-0-2.

3.2.4 Methylation analysis

The structure of polysaccharides could be studied by methylation analysis results, which was considered a potential method widely utilized in the determination of the monosaccharide residues linkages in polysaccharides and oligosaccharides[28]. Methylation analysis for PEP-0.1-1, PEP-0-1 and PEP-0-2 were shown in Table 1. The GC chromatograms of fragments and MS spectra of each corresponding fragment were shown in Fig. S2. Two main linkages were shown in PEP-0.1-1 and the main residue species was glucose (93.37%), with Glc*p*-1, Glc*p*-1-4 and Glc*p*-1-4-6 links. This was followed by galactose (6.63%), which had Gal*p*-1-3-4 link. Nevertheless, 9 main linkages were found in PEP-0-1 whereby main residue specie was glucose (94.2%), with links, t-Glc*p* (18.91%), 3-Glc*p* (11.05%), 6-Glc*p* (1.93%), 4-Glc*p* (51.49%), 3,4-Glc*p* (1.44%), 3,6-Glc*p* (4.60%) and 4,6-Glc*p* (6.60%). Furthermore, PEP-0-1 contained 6-Man*p* (3.08%), and a small amount of 6-Gal*p* (0.89%). In summary, methylation analysis of the 3 polysaccharides were consistent with the above monosaccharide composition results. Nonetheless, the data demonstrated that PEP-0-2 had 10 sugar linkages, which were listed in Table 1.

3.2.5 1D and 2D NMR analysis of PEP-0.1-1, PEP-0-1 and PEP-0-2

For PEP-0.1-1, 6 anomeric proton signals at δ 5.32, 4.89, 5.26, 4.86, 5.15 and 4.57 were observed based on ^{1}H NMR (Fig. S1A-a), ^{13}C NMR (Fig. S1A-b), and cross-peak in HSQC (Fig. 6A$_3$) spectrum, indicating that six monosaccharide residues might be present, which were subsequently labelled A, B, C, D, R_α and R_β respectively. Moreover, the related anomeric carbon signals were at δ 101.14, 99.88, 101.33, 100.06, 93.33 and 97.01 respectively. DEPT-135 (Fig. S1A-d) analysis showed signals at δ 61.97 and 69.17, indicating the presence of $^{-}CH_2$ and a bond at C-6 position.

In addition, chemical shifts of H-1 of residues A, B, C, D, R_α and R_β were derived and assigned using ^{1}H NMR spectrum. Nevertheless, the signals from H-2 to H-5 of residues A, B, D, R_α and R_β were observed through the COSY spectrum (Fig. 6A$_1$) cross peaks while that of H-5 of residue C, and signals of H-6a and H-6b of residues A, B, C, D, R_α and R_β were obtained by HSQC correlation spectrum. The chemical shift of C-1 to C-6 of residues A, B, C, D, R_α and R_β on the sugar ring was also obtained through HSQC correlation spectrum. It was worth mentioning that chemical shift of C-6 of R_α (δ 61.67) and R_β (δ 61.67) could be observed in ^{13}C-NMR and DEPT-135 spectra. Markedly, the chemical shift of C-1, C-4 and C-6 of residue B, C-1 of residue C, C-1, C-3 and C-4 of residue D, C-4 of residue R_α and residue R_β shifted to a lower field, suggesting that the residues were substituted at these positions. Detailed chemical shifts were displayed in Table 2. Combined with HSQC, HMBC (Fig. 6A$_2$), NOESY (Fig. 6A$_4$) spectra, methylation results and findings from other studies[29-30], residues A, B, C, D, R_α and R_β were inferred to be →4)-*α*-*D*-Glc*p*-(1→, →4,6)-*α*-*D*-Glc*p*-(1→, *α*-*D*-Glc*p*-(1→[29-32], →3,4)-*α*-*D*-Glc*p*-(1→[33-34], →4)-*α*-*D*-Glc*p* and →4)-*β*-*D*-Glc*p*[29] respectively.

Table 1
Methylation analysis data for PEP-0.1-1, PEP-0-1 and PEP-0-2.

Sample	RT (min)	Methylated sugar	Mass fragments (*m/z*)	Molar ratios (%)	Type of linkage
PEP-0.1-1	23.822	1,5-di-*O*-acetyl-2,3,4,6-tetra-*O*-methyl glucitol	43, 71, 87, 101, 117, 129, 145, 161, 205	17.71	1-Glc*p*
	29.570	1,4,5-tri-*O*-2,3,6-tri-*O*- methyl glucitol	43, 71, 87, 99, 101, 113, 117, 129, 131, 161, 173, 233	65.51	1,4-Glc*p*
	33.546	1,3,4,5-tetra-*O*-acetyl-2,6-di-*O*-methyl glucitol	43, 87, 97, 117, 129, 143, 159, 185	6.63	1,3,4-Gal*p*
	36.476	1,4,5,6-tetra-*O*-acetyl-2,3-di-*O*-methyl glucitol	43, 85, 99, 101, 117, 127, 142, 159, 201, 261	10.15	1,4,6-Glcp
PEP-0-1	8.779	1,5-di-*O*-acetyl-2,3,4,6-tetra-*O*-methyl glucitol	59, 71, 87, 102, 129, 145, 162, 189, 205, 239	18.912	t-Glc*p*
	11.987	1,3,5-tri-*O*-acetyl-2,4,6-tri-*O*-methyl glucitol	76, 101, 117, 149, 165, 190, 223	11.054	3-Glc*p*
	13.347	1,5,6-tri-*O*-acetyl-2,3,4-tri-*O*-methyl mannitol	59, 87, 101, 118, 160, 174, 203, 234, 264	13.347	6-Man*p*
	13.466	1,5,6-tri-*O*-acetyl-2,3,4-tri-*O*-methyl glucitol	73, 87, 102, 129, 143, 162, 189, 218, 233	13.466	6-Glc*p*
	14.040	1,4,5-tri-*O*-acetyl-2,3,6-tri-*O*-methyl glucitol	71, 87, 118, 162, 191, 233, 277	14.04	4-Glc*p*
	15.200	1,5,6-tri-*O*-acetyl-2,3,4-tri-*O*-methyl galactitol	71, 87, 102, 118, 162, 189, 203, 233	15.2	6-Gal*p*
	15.978	1,3,4,5-tetra-*O*-acetyl-2,6-di-*O*-methyl glucitol	55, 69, 83, 97, 122, 150, 178, 206, 234, 262, 290, 319	15.978	3,4-Glc*p*
	17.524	1,3,5,6-tetra-*O*-acetyl-2,4-di-*O*-methyl glucitol	59, 87, 101, 118, 160, 189, 202, 234, 305	17.524	3,6-Glc*p*
	18.116	1,4,5,6-tetra-*O*-acetyl-2,3-di-*O*-methyl glucitol	74, 102, 118, 142, 201, 231, 261, 305	18.116	4,6-Glc*p*
PEP-0-2	8.614	1,5-di-*O*-acetyl-2,3,4,6-tetra-*O*-methyl mannitol	59, 71, 87, 102, 129, 145, 205, 239	6.418	t-Man*p*
	8.700	1,5-di-*O*-acetyl-2,3,4,6-tetra-*O*-methyl glucitol	59, 71, 87, 102, 118, 145, 162, 205, 239	15.778	t-Glc*p*
	11.908	1,3,5-tri-*O*-acetyl-2,4,6-tri-*O*-methyl glucitol	59, 87, 101, 118, 143, 161, 174, 203, 234, 277	5.632	3-Glc*p*
	13.333	1,5,6-tri-*O*-acetyl-2,3,4-tri-*O*-methyl mannitol	73, 101, 118, 160, 202, 234, 284, 338	3.106	6-Man*p*
	13.444	1,5,6-tri-*O*-acetyl-2,3,4-tri-*O*-methyl glucitol	71, 88, 99, 131, 162, 191, 204, 234	2.034	6-Glc*p*
	13.821	1,4,5-tri-*O*-acetyl-2,3,6-tri-*O*-methyl glucitol	71, 87, 118, 162, 191, 233, 277	37.981	4-Glc*p*
	15.192	1,5,6-tri-*O*-acetyl-2,3,4-tri-*O*-methyl galactitol	71, 87, 102, 118, 162, 189, 204, 233	11.728	6-Gal*p*
	17.463	1,3,5,6-tetra-*O*-acetyl-2,4-di-*O*-methyl mannitol	59, 87, 101, 118, 160, 189, 202, 234, 305	2.951	3,6-Man*p*
	18.034	1,4,5,6-tetra-*O*-acetyl-2,3-di-*O*-methyl glucitol	74, 102, 118, 142, 201, 231, 261	5.591	4,6-Glc*p*
	19.355	1,2,5,6-tetra-*O*-acetyl-3,4-di-*O*-methyl galactitol	74, 87, 114, 130, 159, 190, 234	8.781	2,6-Gal*p*

Table 2
^{1}H and ^{13}C NMR chemical shifts of PEP-0.1-1 in D_2O.

Glycosyl residues			Chemical shift (δ)						
			1	2	3	4	5	6a	6b
A	→4)-*α*-*D*-Glc*p*-(1→	H	5.32	3.55	3.9	3.58	3.78	3.79	3.71
		C	101.14	72.91	74.56	78.31	72.53	61.89	
B	→4,6)-*α*-*D*-Glc*p*-(1→	H	4.89	3.49	3.67	3.36	3.57	3.79	3.89
		C	99.88	72.86	74.02	77.1	70.69	68.46	
C	*α*-*D*-Glc*p*-(1→	H	5.26	3.55	3.67	3.38	3.68	3.85	3.90
		C	101.33	73.07	74.13	70.71	74.2	64.3	
D	→3,4)-*α*-*D*-Glc*p*-(1→	H	4.86	3.51	4.15	3.66	3.78	3.77	
		C	100.16	73.18	76.58	77.71	72.69	61.78	
R_α	→4)-*α*-*D*-Glc*p*	H	5.15	3.48	3.9	3.55	3.77	3.79	3.7
		C	93.33	72.8	77.4	79.52	72.11	61.67	
R_β	→4)-*β*-*D*-Glc*p*	H	4.57	3.19	3.7	3.77	3.58	3.79	3.7
		C	97.01	75.56	77.5	78.39	74.99	61.67	

In the NOESY spectrum, there was a cross peak between H-1 (δ 5.32) and H-4 (δ 3.58) of residue A, between H-1 (δ 4.89) of A and H-4 (δ 3.58) of B, between H-1 (δ 5.32) of A and H-4 (δ 3.36) of B, between H-1 (δ 5.32) of A and H-4 (δ 3.66) of D, H-1 (δ 5.26) of C and H-6 (δ 3.79) of B and between H-1 (δ 4.86) of D and H-4 (δ 3.58) of A. However, residues, R_α and R_β showed no cross signal in HMBC correlation and NOESY spectra since their content was minimal. Combined with methylation analysis results, the molar ratio of residues A, B, C and D was 6:1:2:1, respectively, which demonstrated that the purified fractions were composed of residues A and B connected by 1-4 glycosidic bonds to form a sugar backbone with two reducing end groups. The preliminary structure of the polysaccharide sample (PEP-0.1-1) was, →4)-*α*-*D*-Glc*p*-(1→ main chain of glucan, *α*-*D*-Glc*p*-(1→ connected to the 6th and the 3rd positions, and contained →4)-*α*-*D*-Glc*p* and →4)-*β*-*D*-Glc*p*. Thus, the possible structure was shown in Fig. 7A.

For PEP-0-1, based on ^{1}H spectrum (Fig. S1B-a), ^{13}C spectrum (Fig. S1B-b), and HSQC (Fig. 6B$_3$) spectrum, several anomeric proton signals at δ 4.85, 4.97, 4.64, 5.25, 5.17, 5.21, 5.24 and 5.22 were detected, respectively, indicating that 8 monosaccharide residues might have been present, labelled as residues A, B, C, D, E, F, G and H, respectively. Basically, related anomeric carbon signals were considered at δ 97.78, 98.16, 101.72, 99.75, 99.53, 99.75, 99.75 and 99.75, respectively. The above chemical shifts of the iso-headed protons and iso-headed carbons indicated that residues A, B, D, E, F, G and H had *α*-configuration and residue C had a *β*-configuration. Additionally, specific chemical shifts of H-1 of residues A, B, C, D, E, F, G and H were derived and assigned using ^{1}H NMR spectrum. The signals from H-2 to H-6 of residues A, B, C, D, E, F, G and H were identified through the COSY spectrum (Fig. 6B$_1$) cross peaks. In addition, the chemical shift of C-1 to C-6 of residues A, B, C, D, E, F, G and H on the sugar ring were determined by HSQC correlation spectrum. Detailed chemical shifts were shown in Table 3. Based on the spectrum, C-1 and C-6 of residue A, C-1, C-2 and C-6 of residue B, C-1 of residue C and E, C-1 and C-4 of residue D, C-1, C-4 and C-6 of residue F and C-1 and C-3 of residue G shifted to a lower field, indicating that the residues were substituted at these positions. Noteworthy, through HSQC and HMBC (Fig. 6B$_2$) spectra, it was shown that the C-3 position was connected to -OMe, the methyl C signal was attributed to δ 56.00, and that the H signal was attributed to δ 3.29. Furthermore, combined with HSQC, HMBC and NOESY spectra (Fig. 6B$_4$), it was shown that the residues A, B, C, D, E, F, G and H were inferred to be →6)-*α*-3-*O*-Me-*D*-Gal*p*-(1→, →2,6)-*α*-*D*-

Gal*p*-(1→, *β*-*D*-Man*p*-(1→[35-37], →4)-*α*-*D*-Glc*p*-(1→, *α*-*D*-Glc*p*-(1→, →4,6)-*α*-*D*-Glc*p*-(1→[38-39], →3)-*α*-*D*-Glc*p*-(1→ and →3,6)-*α*-*D*-Glc*p*-(1→[40], respectively. Additionally, through the coupling signals of hetero-headed hydrogen and carbon on each sugar residue in HMBC spectrum, or through the coupling signals of hetero-headed carbon and hydrogen, the interconnecting sequence between each sugar residue could further be inferred. There were a couple signals between H-1 (*δ* 5.25) and C-4 (*δ* 76.94) of residue D, between H-1 (*δ* 5.24) of G and C-3 (*δ* 78.50) of H, between H-1 (*δ* 5.17) of E and C-3 (*δ* 76.55) of G, between H-1 (*δ* 5.25) of D and C-4 (*δ* 76.94) of F, between C-1 (*δ* 99.75) of H and H-6 (*δ* 3.69) of F and between C-1 (*δ* 101.72) of C and H-2 (*δ* 3.79) of B.

Table 3
^{1}H and ^{13}C NMR chemical shifts of PEP-0-1 in D_2O.

Glycosyl residues			Chemical shift (*δ*)							CH_3 of OMe
			1	2	3	4	5	6a	6b	
A	→6)-*α*-3-*O*-Me-*D*-Gal*p*-(1→	H	4.85	3.71	3.40	4.15	4.05	3.55	3.79	3.29
		C	97.78	69.27	78.97	65.49	68.83	66.69		56
B	→2,6)-*α*-*D*-Gal*p*-(1→	H	4.97	3.79	3.60	3.97	3.86	3.54	3.78	
		C	98.16	77.14	73.00	69.05	68.83	66.68		
C	*β*-*D*-Man*p*-(1→	H	4.64	3.95	3.50	3.40	3.23	3.60	3.78	
		C	101.72	70.26	72.61	71.63	75.57	60.94		
D	→4)-*α*-*D*-Glc*p*-(1→	H	5.25	3.45	3.84	3.51	3.68	3.69	3.76	
		C	99.75	71.50	73.35	76.94	70.80	60.34		
E	*α*-*D*-Glc*p*-(1→	H	5.17	3.37	3.89	3.52	4.05	3.75	3.67	
		C	99.53	71.41	70.03	70.42	68.67	60.75		
F	→4,6)-*α*-*D*-Glc*p*-(1→	H	5.21	3.53	3.80	3.51	3.55	3.69		
		C	99.75	73.22	70.64	76.94	72.76	68.54		
G	→3)-*α*-*D*-Glc*p*-(1→	H	5.24	3.46	3.60	3.26	3.58	3.80	3.59	
		C	99.75	71.60	76.55	69.40	72.76	61.03		
H	→3,6)-*α*-*D*-Glc*p*-(1→	H	5.22	3.46	3.49	3.26	–	3.77		
		C	99.75	71.60	78.50	69.40	–	68.75		

Note: "–" indicates no signal was detected.

Further, in the NOESY spectrum, there was a cross peak between H-1 and H-4 of residue D, suggesting that residue D was self-linked by a *α*-1,4-glycosidic bond. There was also a cross peak between H-1 of H and H-4 of F, between H-1 of B and H-6 of A, between H-1 of A and H-6 of B and H-1 of C and H-2 of B. Consequently, these results showed that residue H was connected to F by a *α*-1,4-glycosidic bond, residue B to A by a *α*-1,6-glycosidic bond, residue A to residue B by a *α*-1,6-glycosidic bond and residue C was connected to residue B by a *β*-1,2 glycosidic bond.

In HMBC and HSQC spectra, no cross peaks were observed between residues D, E, F, G, H and A, B, C. In addition, based on molecular weight results, it was noted that there might have been two types of repeated structural units in the samples. Hence, combined with the methylation analysis results above, the ratio of residues D:F:G:H was close to 10:1:2:1. Consequently, the possible structure for PEP-0-1 was shown in Fig. 7B.

For PEP-0-2, based on ^{1}H NMR (Fig. S1C-a), ^{13}C NMR (Fig. S1C-b), and cross-peak in HSQC (Fig. 6C$_3$) spectra, 6 anomeric proton signals at *δ* 4.85, 4.97, 4.64, 5.25, 5.17 and 5.22 were shown, indicating that six monosaccharide residues might have been present, which were subsequently labelled A, B, C, D, E and F respectively. The related anomeric carbon signals were at *δ* 97.78, 98.16, 101.72, 99.75, 99.53 and 99.75, respectively and the chemical shifts for residues A, B, D, E and F had *α*-configuration, and *β*-configuration for residue C. The chemical shifts for H-1 of residues A, B, C, D, E and F were derived and assigned using ^{1}H NMR. On the other hand, the signals from H-2 to H-6 of residues A, B, C and D, H-2 to H-5 of residue E and from H-2 to H-4 of residue F were identified through the COSY spectrum (Fig. 6C$_1$) cross peaks. Further, signals from H-6a and H-6b of residue E were affirmed through the HSQC spectrum. Hence, for residue F, H-5 signal was too weak to be detected. Nonetheless, H-6 signal was attributed to *δ* 3.71 through HSQC spectrum. Noticeably, C-3 position of residue A was connected to −OMe, residue C signal was attributed to *δ* 56.00, and that of H was attributed to *δ* 3.29. Detailed chemical shifts were shown in Table 4. The chemical shift for C-1 and C-6 of residue A, C-1、C-2 and C-6 of residue B, C-1 of residue C, C-1, C-1 and C-4 of residue D, C-1 of residue E and C-1, C-4 and C-6 of residue F shifted to a lower field, indicating that the residues were substituted at these positions. Combined with HSQC, HMBC (Fig. 6C$_2$) and NOESY spectra (Fig. 6C$_4$), residues A, B, C, D, E and F were inferred to be →6)-*α*-3-*O*-Me-*D*-Gal*p*-(1→, →2,6)-*α*-*D*-Gal*p*-(1→, *β*-*D*-Man*p*-(1→[35-37], →4)-*α*-*D*-Glc*p*-(1→, *α*-*D*-Glc*p*-(1→ and →4,6)-*α*-*D*-Glc*p*-(1→, respectively[38-39].

Table 4
^{1}H and ^{13}C NMR chemical shifts of PEP-0-2 in D_2O.

Glycosyl residues			Chemical shift (*δ*)							CH_3 of OMe
			1	2	3	4	5	6a	6b	
A	→6)-*α*-3-*O*-Me-*D*-Gal*p*-(1→	H	4.85	3.71	3.40	4.15	4.05	3.55	3.79	3.29
		C	97.78	69.27	78.97	65.49	68.83	66.69		56
B	→2,6)-*α*-*D*-Gal*p*-(1→	H	4.97	3.79	3.60	3.97	3.86	3.54	3.78	
		C	98.16	77.14	73.00	69.05	68.83	66.68		
C	*β*-*D*-Man*p*-(1→	H	4.64	3.95	3.50	3.40	3.23	3.60	3.78	
		C	101.72	70.26	72.61	71.63	75.57	60.94		
D	→4)-*α*-*D*-Glc*p*-(1→	H	5.25	3.45	3.84	3.52	3.68	3.69	3.76	
		C	99.75	66.47	71.24	77.77	70.80	60.34		
E	*α*-*D*-Glc*p*-(1→	H	5.17	3.37	3.89	3.52	4.05	3.75	3.67	
		C	99.53	71.41	70.03	70.42	68.67	60.75		
F	→4,6)-*α*-*D*-Glc*p*-(1→	H	5.22	3.63	3.93	3.49	–	3.71		
		C	99.75	73.22	70.64	76.50	–	67.08		

Note: "–" indicates no signal was detected.

Besides, a number of signals were observed between H-1 (*δ* 4.97) of residue B and C-6 (*δ* 66.69) of residue A, H-1 (*δ* 4.85) of A and C-6 (*δ* 66.68) of B, between H-1 (*δ* 4.64) of C and C-2 (*δ* 77.14) of B, and between C-1 (*δ* 101.72) of C and H-2 (*δ* 3.79) of B.

In NOESY spectrum, there was a cross peak between H-1 and H-4 of residue D, demonstrating that the residue was self-linked by a *α*-1,4-glycosidic bond. There was also a cross peak between H-1 of D and H-4 of F, between H-1 of E and H-6 of F, between H-1 of B and H-6 of A, between H-1 of A and H-6 of B and between H-1 of C and H-6 of B, indicating that residue D was connected to F by a *α*-1,4-glycosidic bond. Moreover, from the spectrum, residue E was connected to F by *α*-1,6-glycosidic bond, residue B to residue A by a *α*-1,6-glycosidic bond, A to B by a *α*-1,6-glycosidic bond and residue C was connected to residue B by a *β*-1,2 glycosidic bond.

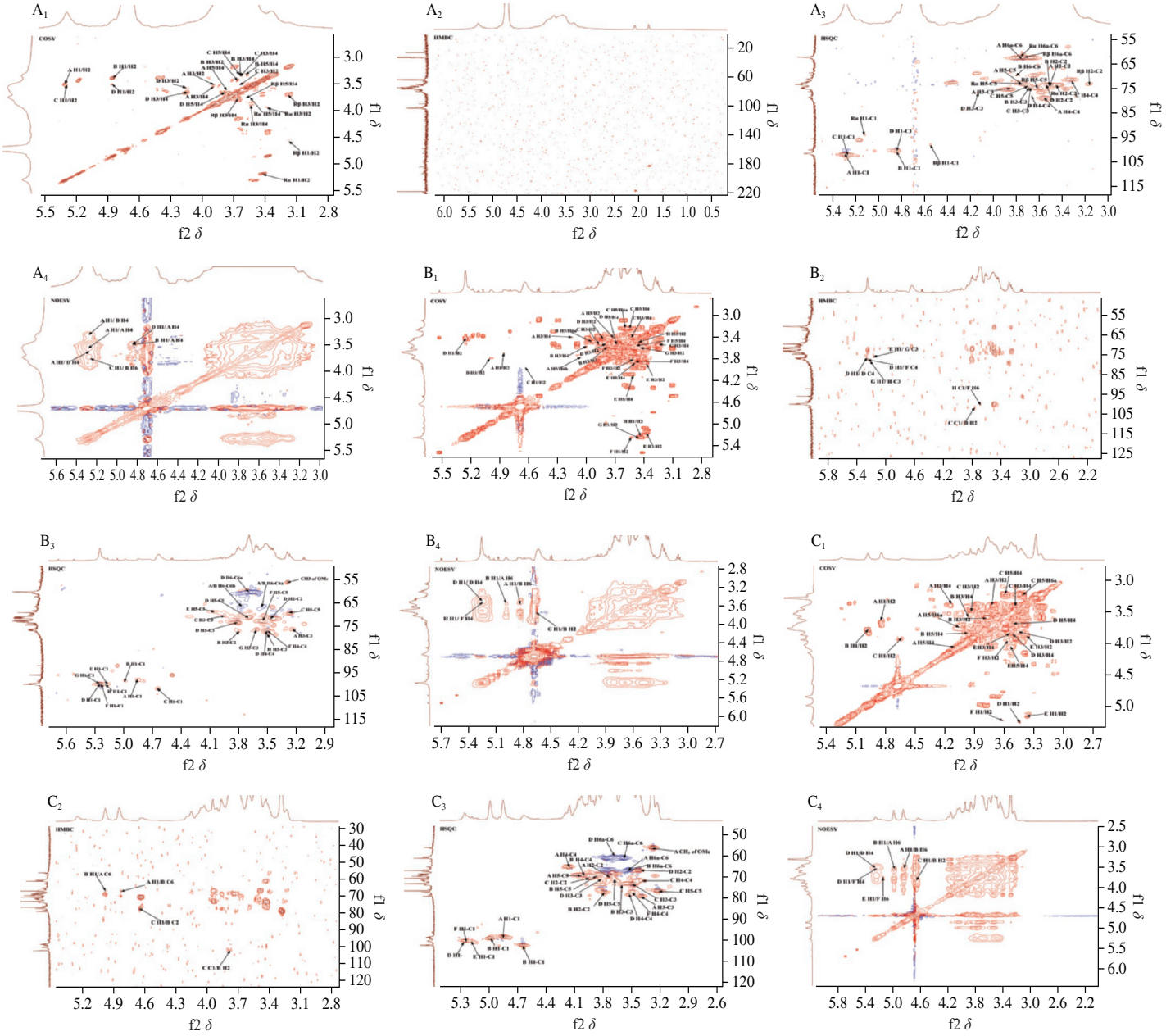

Fig. 6 NMR spectrum of (A) PEP-0.1-1, (B) PEP-0-1 and (C) PEP-0-2 in D2O. (A_1, B_1, C_1) COSY, (A_2, B_2, C_2) HMBC, (A_3, B_3, C_3) HSQC and (A_4, B_4, C_4) NOESY spectra.

In HMBC and HSQC spectra, there was no cross peak between residues D, E, F and A, B, C. Nonetheless, according to molecular weight results, it was speculated that there might have been two types of repeated structural units in the samples. Combined with the above results, the molar ratio of residues A to B was close to 4:3 while that of residue D to F was close to 7:1 respectively. As a result, the possible structure for PEP-0-2 was illustrated in Fig. 7C.

3.3 Inhibitory effects of purified P. eryngii polysaccharides on LPS-induced inflammation of RAW264.7 cells

The effect of purified polysaccharides, PEP-0.1-1, PEP-0-1 and PEP-0-2 on RAW264.7 cells activity was determined by CCK-8 kit. The 3 polysaccharides had no toxicity on RAW264.7 cells at a concentration of 5, 10 and 25 μg/mL as shown in Fig. 8A. In order to reveal the anti-inflammatory effects from mRNA and protein level, RT-PCR, as well as ELASA methods were utilized in the present study to reveal the cytokines production and secretion of inflammation cytokines, including NO, TLR4, TNF-α, IL-6, and IL-1β. LPS stimulation could lead to overexpression of TLR4, NO, TNF-α, IL-6 and IL-1β related mRNA in macrophages, but polysaccharide intervention could inhibit the overexpression of related mRNA as illustrated in Fig. 8B−F. Significant differences were found for the inhibition effects of these 3 purified polysaccharides on LPS-induced mRNA overexpression in cells at the concentrations of 5, 10 and 25 μg/mL. Notably, at concentration of 25 μg/mL, the 3 polysaccharides exhibited the highest inhibition effect. Inflammation was the body's defensive response, which was usually beneficial to the body, but

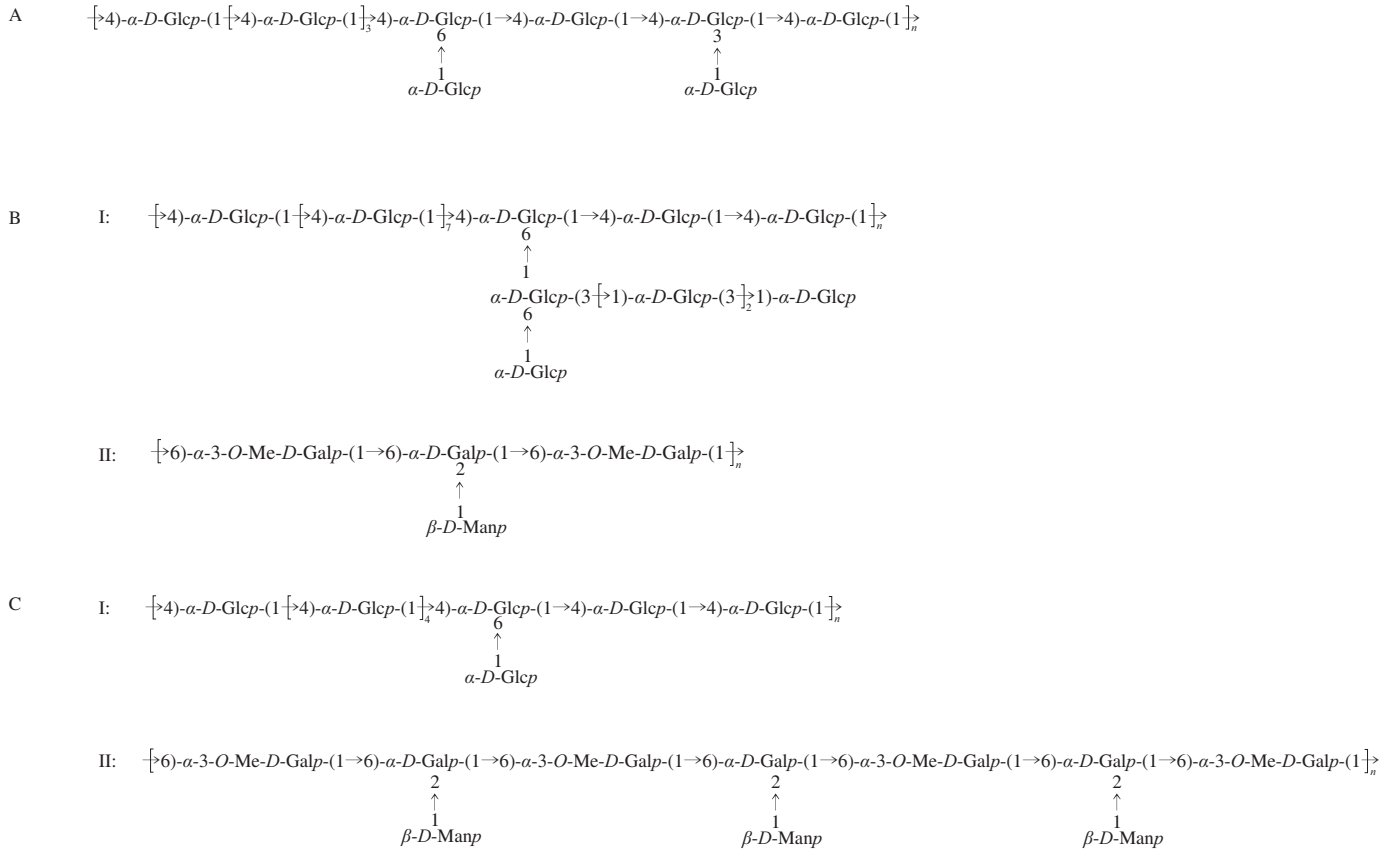

Fig. 7 Putative structures of (A) PEP-0.1-1, (B) PEP-0-1 and (C) PEP-0-2.

excessive inflammation could lead to the secretion of excessive inflammatory cytokines in the host, causing local or systemic inflammatory responses, excessive cytokine production could cause serious cell damage, traditional steroidal anti-inflammatory drugs have more side effects, so we can isolate natural anti-inflammatory preparations from *P. eryngii* that have less side effects on the human body. Herein, a more intuitive anti-inflammatory effect was observed from the ELASA results. Basically, significant inhibition effects were exhibited with the treatment of different purified *P. eryngii* polysaccharides on LPS-induced cell inflammation at the concentration of 5, 10 and 25 μg/mL (Fig. 9), from which the PEP-0.1-1 fraction displayed the most inhibition effects. TLR4 was a receptor on the surface of macrophages, and polysaccharides could activate downstream signaling pathways by binding to TLR4 receptors on the surface of RAW264.7 cells, leading to the secretion of NO and different cytokines (TNF-α, IL-6 and IL-1β). NO was considered the main effector molecule produced by RAW264.7 cells, which has a variety of biological functions and can regulate a variety of cellular functions, such as signal transduction and metabolic regulation, and was considered the main marker of RAW264.7 cell activation. The binding of LPS onto receptor TLR4 stimulates macrophages to secrete excessive amounts of pro-inflammatory factors causing inflammation, which were found mainly TNF-α and multiple interleukins related to nuclear factor κ-B (NF-κB) and mitogen activated protein kinase (MAPK) pathways. Accordingly, a significant anti-inflammatory activity was observed for the three purified *P. eryngii* polysaccharides, suggesting their potential application in the development of novel functional foods.

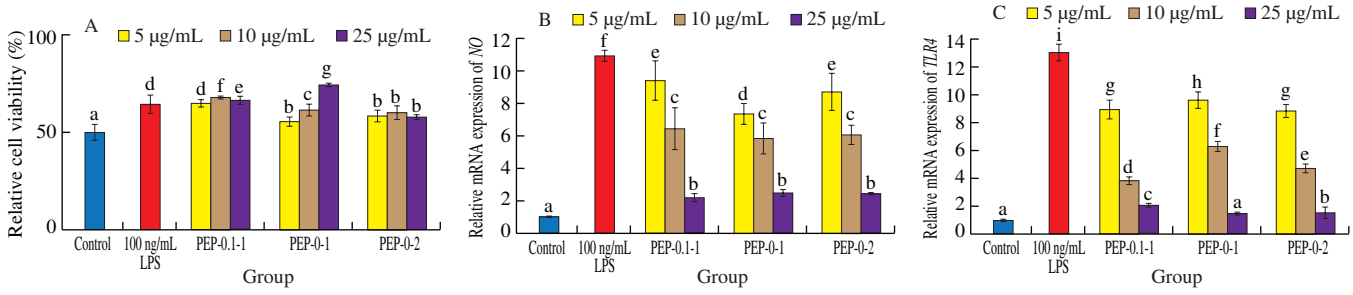

Fig. 8 Cell viability and anti-inflammatory effects of polysaccharides from *P. eryngii* on RAW264.7 cells. The cells were pre-treated with the 3 polysaccharides for 4 h and then treated with LPS at a final concentration of 100 ng/mL for 24 h. (A) Cell viability was determined by CCK-8; Relative mRNA expressions of (B) *NO*, (C) *TLR4*, (D) *TNF-α*, (E) *IL-1β*, and (F) *IL-6*. Different lowercase letters (a-i) represent the statistical difference at $P < 0.05$ among the investigated groups.

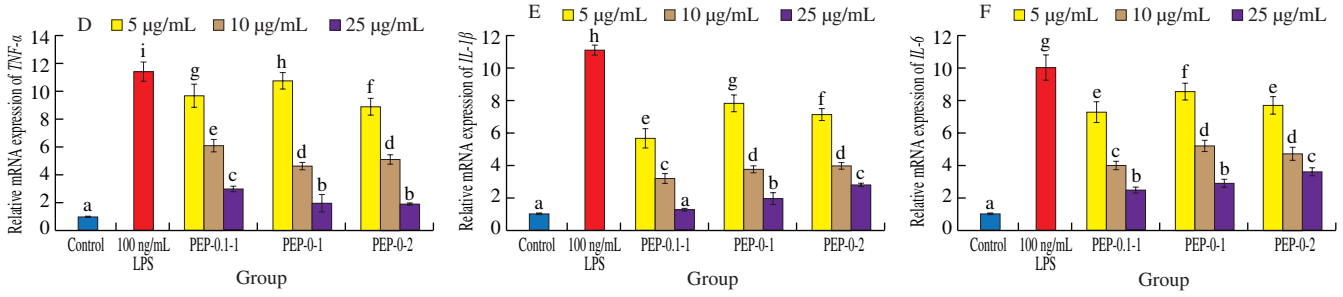

Fig. 8 (*Continued*)

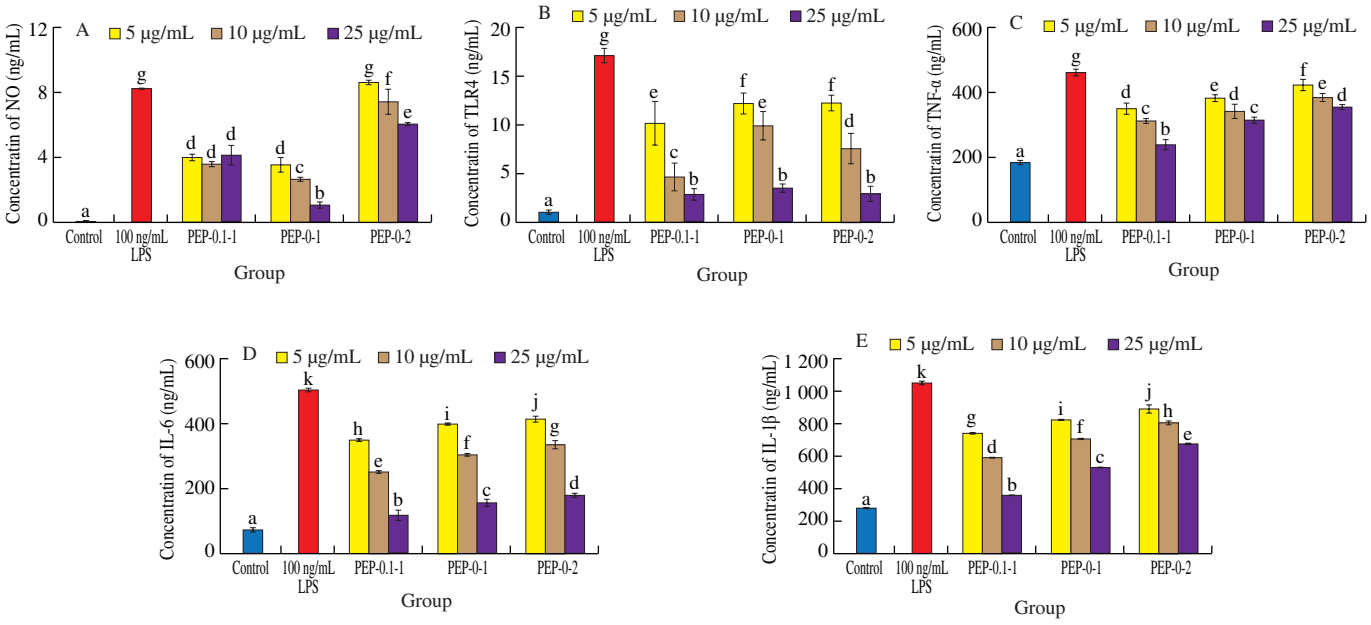

Fig. 9 Inhibitory effects of PEP-0.1-1, PEP-0-1, and PEP-0-2 interfere with macrophages at concentrations of 5, 10, and 25 μg/mL on LPS-induced macrophages (A) NO, (B) TLR4, (C) TNF-α, (D) IL-6 and (E) IL-1β secretion. Different lowercase letters (a–i) indicate statistical difference between different experimental groups ($P < 0.05$).

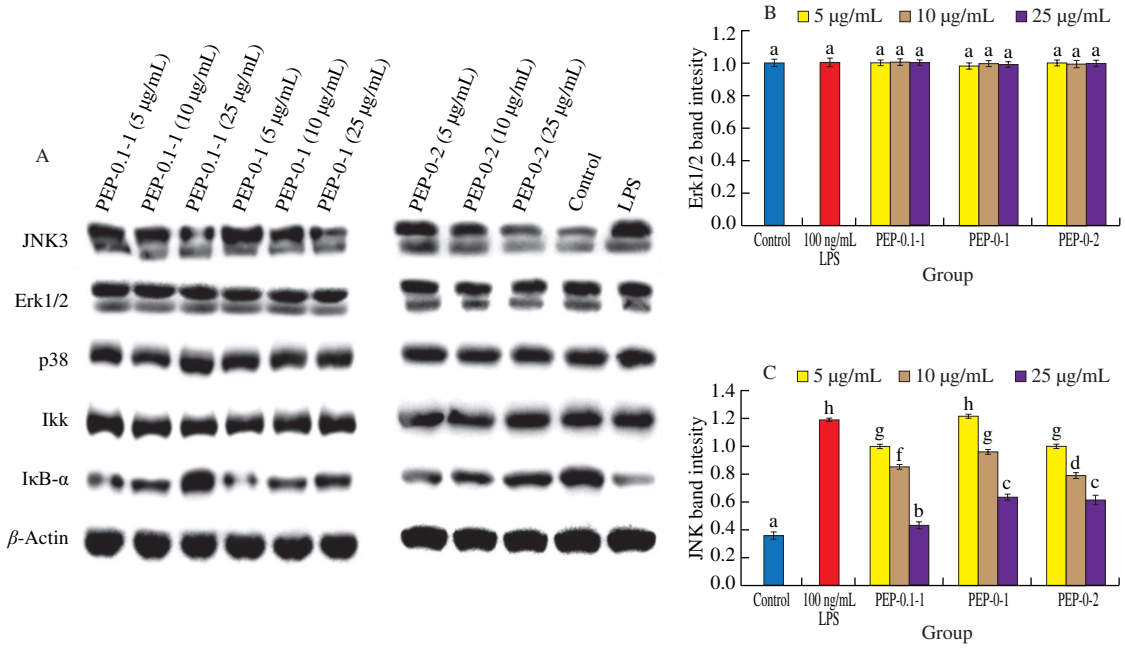

Fig. 10 Effects of PEP-0.1-1, PEP-0-1 and PEP-0-2 on LPS-induced activation of key proteins of MAPK and NF-κB signaling pathways in RAW264.7 cells (different letters indicate statistical differences between different experimental groups, $P < 0.05$).

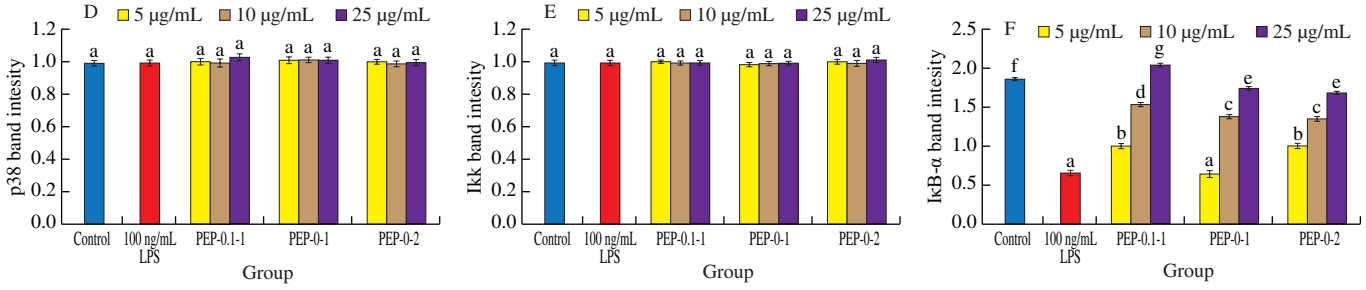

Fig. 10 (*Continued*)

3.4 Regulatory effects of P. eryngii purified polysaccharides on MAPK and NF-κB pathways

NF-κB was considered a eukaryotic transcription factor that can be expressed in a wide range of cells and was a major regulator of natural immunity, adaptive immunity and inflammation[41]. As the major downstream pathway of MAPK signaling, NF-κB was normally phosphorylated after MAPK activation, leading to gene expression of proinflammatory factors[42]. Moreover, the activated NF-κB pathway could induce the expression of *NO*, *IL-1β*, *IL-6* and *TNF-α* related genes. Specifically, IκB-α was proved a key inhibitor of NF-κB, which could inhibit the subunit translocation of key protein p65 in NF-κB pathway. Generally, as the results exhibited, PEP-0.1-1, PEP-0-1, and PEP-0-2 could significantly relieve the inhibitory effect of LPS on IκB-α in RAW264.7 cells at the concentrations of 5, 10, 25 μg/mL. Particularly, with the concentration increased in the range of 5, 10, 25 μg/mL, the disinhibition effects were more significant. On the other hand, no significant effects were observed on the expression of IKK protein in the NF-κB pathway of RAW264.7 under LPS treatment compared with control group (Fig. 10). In summary, PEP-0.1-1, PEP-0-1, and PEP-0-2 could inhibit the increasing expression of JNK in MAPK pathway and decreasing expression of IκB-α in NF-κB pathway induced by LPS stimulation in RAW264.7 cells, which were considered the main approach and reason for the expression of *NO*, *TNF-α*, *IL-6* and *IL-1β* related genes and secretion of NO, TNF-α, IL-6 and IL-1β.

4. Conclusion

In this research, one natural polysaccharide PEP-0.1-1 and 2 neutral polysaccharides PEP-0-1 and PEP-0-2 were isolated, purified and characterized. According to characterization results, PEP-0.1-1 mainly contained 1,4-linked Glc*p* while PEP-0-1 had two main chains and was highly branched. Further, PEP-0-1 backbone mainly contained 1,4-linked Glc*p* and 1,6-linked Gal*p*, with notable methylation on Gla*p*. The backbone of PEP-0-2 was similar to PEP-0-1, while that of PEP-0-2 had few branches. On the other hand, all these polysaccharides displayed significant effects on cell inflammation induced by LPS stimulation in RAW264.7 cells through NF-κB and MAPK signal pathways, which were related to the inhibition on the increasing expression of JNK in MAPK pathway and decreasing expression of IκB-α in NF-κB pathway, which were considered the main approach and reason for the expression of NO, TNF-α, IL-6 and IL-1β related genes and secretion of NO, TNF-α, IL-6 and IL-1β. In conclusion, the findings of the present study showed that the purified polysaccharides obtained from *P. eryngii* could serve as novel natural anti-inflammatory components for the exploitation in functional foods or drugs formulation.

Declaration of competing interest

The authors report no conflicts of interest.

Acknowledgement

This work was supported by the National Natural Science Foundation of China (31901623), Major Public Welfare Projects in Henan Province (201300110200) and the Priority Academic Program Development of Jiangsu Higher Education Institutions (PAPD).

Appendix A. Supplementary data

Supplementary data associated with this article can be found, in the online version, at http://doi.org/10.26599/FSHW.2022.9250245.

References

[1] F. Motta, M.E. Gershwin, C. Selmi., Mushrooms and immunity, J. Autoimmun. 117 (2021) 102576. http://dx.doi.org/10.1016/j.jaut.2020.102576.

[2] X.L. Ji, Y.Q. Cheng, J.Y. Tian, et al., Structural characterization of polysaccharide from jujube (*Ziziphus jujuba* Mill.) fruit, Chem. Biol. Technol. Agric. 8(1) (2021). http://doi.org/10.1186/s40538-021-00255-2.

[3] S. Li, N.P. Shah, Characterization, antioxidative and bifidogenic effects of polysaccharides from *Pleurotus eryngii* after heat treatments, Food Chem. 197 (2016) 240-249. http://dx.doi.org/10.1016/j.foodchem.2015.10.113.

[4] I. Roncero-Ramos, C. Delgado-Andrade, The beneficial role of edible mushrooms in human health, Curr. Opin. Food Sci. 14 (2017) 122-128. http://dx.doi.org/10.1016/j.cofs.2017.04.002.

[5] P. Maity, I.K. Sen, I. Chakraborty, et al., Biologically active polysaccharide from edible mushrooms: a review, Int. J. Biol. Macromol. 172 (2021) 408-417. http://doi.org/10.1016/j.ijbiomac.2021.01.081.

[6] S. Teniou, A. Bensegueni, B.M. Hybertson, et al., Biodriven investigation of the wild edible mushroom *Pleurotus eryngii* revealing unique properties as functional food, J. Funct. Foods 89 (2022) 104965. http://dx.doi.org/10.1016/j.jff.2022.104965.

[7] C.F. Ellefsen, C.W. Wold, A.L. Wilkins, et al., Water-soluble polysaccharides from *Pleurotus eryngii* fruiting bodies, their activity and affinity for Toll-like receptor 2 and dectin-1, Carbohydr. Polym. 264 (2021) 117991. http://dx.doi.org/10.1016/j.carbpol.2021.117991.

[8] H.L. Liu, T.H. Kao, C.Y. Shiau, et al., Functional components in *Scutellaria barbata* D. Don with anti-inflammatory activity on RAW 264.7 cells, J. Food Drug Anal. 26(1) (2018) 31-40. http://dx.doi.org/10.1016/j.jfda.2016.11.022.

[9] F. Jiang, Y.Y. Ding, Y. Tian, et al., Hydrolyzed low-molecular-weight polysaccharide from *Enteromorpha prolifera* exhibits high anti-inflammatory activity and promotes wound healing, Mat Sci Eng C-Mater. (2021) 112637. http://dx.doi.org/10.1016/j.msec.2021.112637.

[10] C.Y. Hou, L.L. Chen, L.Z. Yang, et al., An insight into anti-inflammatory effects of natural polysaccharides, Int. J. Biol. Macromol. 153 (2020) 248-255. http://dx.doi.org/10.1016/j.ijbiomac.2020.02.315.

[11] S.J. Li, Y.L. Wu, H.T. Jiang, et al., Chicory polysaccharides alleviate high-fat diet-induced non-alcoholic fatty liver disease via alteration of lipid metabolism- and inflammation-related gene expression, Food Sci. Hum. Wellness. 11(4) (2022) 954-964. http://dx.doi.org/10.1016/j.fshw.2022.03.025.

[12] S. Li, N.P. Shah, Anti-inflammatory and anti-proliferative activities of natural and sulphonated polysaccharides from *Pleurotus eryngii*, J. Funct. Foods 23 (2016) 80-86. http://dx.doi.org/10.1016/j.jff.2016.02.003.

[13] M.L.L. Silveira, F.R. Smiderle, F. Agostini, et al., Exopolysaccharide produced by *Pleurotus sajor-caju*: its chemical structure and anti-inflammatory activity, Int. J. Biol. Macromol. 75 (2015) 90-96. http://dx.doi.org/10.1016/j.ijbiomac.2015.01.023.

[14] D. Morales, F.R. Smiderle, M. Villalva, et al., Testing the effect of combining innovative extraction technologies on the biological activities of obtained *β*-glucan-enriched fractions from *Lentinula edodes*, J. Funct. Foods 60 (2019) 103446. http://dx.doi.org/10.1016/j.jff.2019.103446.

[15] B.R. Zhang, Y.Y. Li, F.M. Zhang, et al., Extraction, structure and bioactivities of the polysaccharides from *Pleurotus eryngii*: a review, Int. J. Biol. Macromol. 150 (2020) 1342-1347. http://doi.org10.1016/j.ijbiomac.2019.10.144.

[16] Y. Song, J. Zhao, Y.Y. Ni, et al., Solution properties of a heteropolysaccharide extracted from pumpkin (*Cucurbita pepo*, lady godiva), Carbohydr. Polym. 132 (2015) 221-227. http://dx.doi.org/10.1016/j.carbpol.2015.06.061.

[17] E. Wei, R. Yang, H. Zhao, et al., Microwave-assisted extraction releases the antioxidant polysaccharides from seabuckthorn (*Hippophae rhamnoides* L.) berries, Int. J. Biol. Macromol. 123 (2019) 280-290. http://dx.doi.org/10.1016/j.ijbiomac.2018.11.074.

[18] M. Kim, S.R. Kim, J. Park, et al., Structure and antiviral activity of a pectic polysaccharide from the root of *Sanguisorba officinalis* against enterovirus 71 *in vitro*/*vivo*, Carbohydr. Polym. 281 (2022) 119057. http://dx.doi.org/10.1016/j.carbpol.2021.119057.

[19] G. Ma, Q. Xu, H. Du, et al., Characterization of polysaccharide from *Pleurotus eryngii* during simulated gastrointestinal digestion and fermentation, Food Chem. 370 (2022) 131303. http://dx.doi.org/10.1016/j.foodchem.2021.131303.

[20] D. Morales, F.R. Smiderle, M. Villalva, et al., Testing the effect of combining innovative extraction technologies on the biological activities of obtained *β*-glucan-enriched fractions from *Lentinula edodes*, J. Funct. Foods 60 (2019) 103446. http://.doi.org/10.1016/j.jff.2019.103446.

[21] X.J. Li, Q. Chen, G.K. Liu, et al., Chemical elucidation of an arabinogalactan from rhizome of Polygonatum sibiricum with antioxidant activities, Int. J. Biol. Macromol. 190 (2021) 730-738. http://dx.doi.org/10.1016/j.ijbiomac.2021.09.038.

[22] F. Li, Y.L. Wei, L. Liang, et al., A novel low-molecular-mass pumpkin polysaccharide: structural characterization, antioxidant activity, and hypoglycemic potential, Carbohydr. Polym. 251 (2021) 117090. http://dx.doi.org/10.1016/j.carbpol.2020.117090.

[23] H. Zhang, P. Zou, H.T. Zhao, et al., Isolation, purification, structure and antioxidant activity of polysaccharide from pinecones of *Pinus koraiensis*, Carbohydr. Polym. 251 (2021) 117078. http://doi.org/10.1016/j.carbpol.2020.117078.

[24] S.N. Wang, L.L. Zhao, Q.H. Li, et al., Rheological properties and chain conformation of soy hull water-soluble polysaccharide fractions obtained by gradient alcohol precipitation, Food Hydrocoll. 91 (2019) 34-39. http://dx.doi.org/10.1016/j.foodhyd.2018.12.054.

[25] H.M. Saleh, M.S.M. Annuar, K. Simarani, Ultrasound degradation of xanthan polymer in aqueous solution: Its scission mechanism and the effect of NaCl incorporation, Ultrason. Sonochem. 39 (2017) 250-261. http://dx.doi.org/10.1016/j.ultsonch.2017.04.038.

[26] Z.K. Muhidinov, J.T. Bobokalonov, I.B. Ismoilov, et al., Characterization of two types of polysaccharides from *Eremurus hissaricus* roots growing in Tajikistan, Food Hydrocoll. 105 (2020) 117090. http://doi.org/10.1016/j.foodhyd.2020.105768.

[27] Y.N. Jia, Z.H. Xue, Y.J. Wang, et al. Chemical structure and inhibition on alpha-glucosidase of polysaccharides from corn silk by fractional precipitation, Carbohydr. Polym. 252 (2021) 117185. http://doi.org/10.1016/j.carbpol.2020.117185.

[28] Y. Chen, T. Wang, X. Zhang, et al., Structural and immunological studies on the polysaccharide from spores of a medicinal entomogenous fungus *Paecilomyces cicadae*, Carbohydr. Polym. 254 (2021) 117462. http://dx.doi.org/10.1016/j.carbpol.2020.117462.

[29] X.D. Shi, O.Y. Li, J.Y. Yin, et al., Structure identification of *α*-glucans from *Dictyophora echinovolvata* by methylation and 1D/2D NMR spectroscopy, Food Chem. 271 (2019) 338-344. http://dx.doi.org/10.1016/j.foodchem.2018.07.160.

[30] Z. Zhang, L. Guo, A. P. Yan, et al., Fractionation, structure and conformation characterization of polysaccharides from *Anoectochilus roxburghii*, Carbohydr. Polym. 231 (2020) 115688. http://dx.doi.org/10.1016/j.carbpol.2019.115688.

[31] J. Wang, S. Nie, S.W. Cui, et al., Structural characterization and immunostimulatory activity of a glucan from natural *Cordyceps sinensis*, Food Hydrocoll. 67 (2017) 139-147. http://dx.doi.org/10.1016/j.foodhyd.2017.01.010.

[32] J. Liu, F.N. Shang, Z.M. Yang, et al., Structural analysis of a homogeneous polysaccharide from *Achatina fulica*, Int. J. Biol. Macromol. 98 (2017) 786-792. http://dx.doi.org/10.1016/j.ijbiomac.2017.01.149.

[33] J. Ganeshapillai, E. Vinogradov, J. Rousseau, et al., *Clostridium difficile* cell-surface polysaccharides composed of pentaglycosyl and hexaglycosyl phosphate repeating units, Carbohydr. Res. 343(4) (2008) 703-710.http://dx.doi.org/10.1016/j.carres.2008.01.002.

[34] X.M. Zheng, H.Q. Sun, L.R. Wu, et al., Structural characterization and inhibition on *α*-glucosidase of the polysaccharides from fruiting bodies and mycelia of *Pleurotus eryngii*, Int. J. Biol. Macromol. 156 (2020) 1512-1519. http://dx.doi.org/10.1016/j.ijbiomac.2019.11.199.

[35] K. Jahanbin, A. Abbasian, M. Ahang, Isolation, purification and structural characterization of a new water-soluble polysaccharide from *Eremurus stenophyllus* (boiss. & buhse) baker roots, Carbohydr. Polym. 178 (2017) 386-393. http://dx.doi.org/10.1016/j.carbpol.2017.09.058.

[36] E.N. Makarova, E.G. Shakhmatov, Characterization of pectin-xylan-glucan-arabinogalactan proteins complex from Siberian fir *Abies sibirica* Ledeb, Carbohydr. Polym. 260 (2021) 117825. http://dx.doi.org/10.1016/j.carbpol.2021.117825.

[37] A.Q. Zhang, Y. Zhang, J.H. Yang, et al., Structural elucidation of a novel heteropolysaccharide from the fruiting bodies of *Pleurotus eryngii*, Carbohydr. Polym. 92(2) (2013). http://dx.doi.org/10.1016/j.carbpol.2012.11.069.

[38] T. Le Costaouëc, C. Unamunzaga, L. Mantecon, et al., New structural insights into the cell-wall polysaccharide of the diatom *Phaeodactylum tricornutum*, Algal. Res. 26 (2017) 172-179. http://dx.doi.org/10.1016/j.algal.2017.07.021.

[39] Y.B. Wang, P.F. He, L. He, et al., Structural elucidation, antioxidant and immunomodulatory activities of a novel heteropolysaccharide from cultured *Paecilomyces cicadae* (Miquel.) Samson, Carbohydr. Polym. 216 (2019) 270-281. http://dx.doi.org/10.1016/j.carbpol.2019.03.104.

[40] Y.J. Zhu, X.R. Wang, C.L. Zhang, et al., Characterizations of glucose-rich polysaccharides from *Amomum longiligulare* T.L. Wu fruits and their effects on immunogenicities of infectious bursal disease virus VP2 protein, Int. J. Biol. Macromol. 183 (2021) 157484. http://dx.doi.org/10.1016/j.ijbiomac.2021.05.138.

[41] G. Dey, R. Bharti, P.K. Ojha, et al., Therapeutic implication of 'Iturin A' for targeting MD-2/TLR4 complex to overcome angiogenesis and invasion, Cell. Signalling 35 (2017) 24-36. http://dx.doi.org/10.1016/j.cellsig.2017.03.017.

[42] M. Wang, X.B. Yang, J.W. Zhao, et al., Structural characterization and macrophage immunomodulatory activity of a novel polysaccharide from *Smilax glabra* Roxb, Carbohydr. Polym. 156 (2017) 390-402. http://dx.doi.org/10.1016/j.carbpol.2016.09.033.